Fermi surface anomaly and depletion of the Fermi sea in the relativistic Brueckner-Hartree-Fock approximation

M. Jaminon and C. Mahaux
Institut de Physique B5, Université de Liège, 4000 Liège 1, Belgium
(Received 6 September 1989)

The Fermi surface anomaly consists in a variation, localized in the vicinity of the Fermi energy, of the energy derivative of the real part of the nuclear mean field. A quantitative analysis of this anomaly is performed in the framework of the relativistic Brueckner-Hartree-Fock approximation to the mean field in symmetric nuclear matter. The investigation is based on dispersion relations that connect the imaginary to the real part of the Lorentz components of the mean field; its main input is the imaginary part of the relativistic mean field recently calculated by ter Haar and Malfliet from a one-boson-exchange nucleon-nucleon interaction. It is found that the Fermi surface anomaly is very nearly the same as in the nonrelativistic Brueckner-Hartree-Fock approximation. However, the physical origin of the anomaly is quite different in the two cases. Relatedly, the predicted depletion of the Fermi sea is much smaller in the relativistic than in the nonrelativistic description. As a consequence, the rearrangement and renormalization corrections are much smaller in the relativistic than in the nonrelativistic case.

I. INTRODUCTION

Relativistic descriptions of nuclear matter and nuclei yield fair agreement with several empirical properties, in particular the average binding energy per nucleon, the density at saturation, the depth of the mean field, and the spin-orbit coupling.[1] We recently emphasized that different definitions are often used for the effective mass in the relativistic and nonrelativistic approaches; we also drew attention to the fact that in both approaches the quantity that can be identified to the empirical effective mass is enhanced in the vicinity of the Fermi energy if one goes beyond the static Hartree-Fock description.[2] This enhancement has been dubbed the Fermi surface anomaly, see, e.g., Ref. 3. The main purpose of the present paper is threefold. First, we perform a quantitative investigation of this anomaly in the framework of the relativistic Brueckner-Hartree-Fock (BHF) approximation to nuclear matter. Second, we evaluate the depletion of the Fermi sea in this approximation. Third, we perform a crude estimate of those corrections to the mean field that are called the correlation and renormalization contributions in nonrelativistic approaches. Our analysis is based on dispersion relations that connect the real and imaginary parts of the mean field; it uses as main input results calculated by ter Haar and Malfliet.[4]

Our presentation is as follows. In Sec. II, we construct convenient parametrizations of the imaginary part of the scalar and vector Lorentz components of the mean field computed in Ref. 4. In Sec. III, each Lorentz component of the real part of the mean field is expressed as the sum of a Hartree-Fock (HF) type and of a dispersive contribution, and the latter is calculated by means of a subtracted dispersion relation. The HF contribution and the full real part are evaluated in Sec. IV. Various effective masses are evaluated in Sec. V, with particular emphasis on the one that can be identified with the effective mass derived from the phenomenological nonrelativistic shell- and optical-model analyses; we compare our result with the one derived from the nonrelativistic BHF approximation. Section VI is devoted to the depletion of the Fermi sea. In Sec. VII, we perform a rough estimate of the correlation and renormalization corrections to the relativistic BHF approximation. Section VIII contains a summary and our conclusions.

II. PARAMETRIZATION OF THE IMAGINARY PART

A. Definitions

We consider symmetric nuclear matter. As in Ref. 2, we neglect the Lorentz component that involves $\boldsymbol{\gamma}\cdot\mathbf{k}$, which is small. We denote the relativistic mean field by $\mathcal{U}_\sigma(k;\omega)+\gamma_0\mathcal{U}_0(k;\omega)$, where k is the nucleon momentum and ω its frequency. The scalar potential $\mathcal{U}_\sigma$ and the vector potential $\mathcal{U}_0$ are complex:

$$\begin{aligned}\mathcal{U}_\sigma(k;\omega)&=\mathcal{V}_\sigma(k;\omega)+i\mathcal{W}_\sigma(k;\omega)\ ,\\ \mathcal{U}_0(k;\omega)&=\mathcal{V}_0(k;\omega)+i\mathcal{W}_0(k;\omega)\ .\end{aligned}\tag{2.1}$$

The one-body Dirac equation amounts to the following energy-momentum relation ($\hbar=c=1$):

$$[\omega+m-\mathcal{U}_0(k;\omega)]^2=k^2+[m+\mathcal{U}_\sigma(k;\omega)]^2\ .\tag{2.2}$$

The Fermi energy ε_F is the value taken by ω when k is equal to the Fermi momentum k_F. The imaginary parts $\mathcal{W}_\sigma(k;\omega)$ and $\mathcal{W}_0(k;\omega)$ vanish like $(\omega-\varepsilon_F)^2$ for ω close to ε_F. Equation (2.2) can be written in the Schrödinger-type form

$$k^2+2m\,\mathcal{U}_e(k;\omega)=\omega^2+2m\omega\ ;\tag{2.3}$$

$$\mathcal{U}_e(k;\omega)=\mathcal{V}_e(k;\omega)+i\mathcal{W}_e(k;\omega)\tag{2.4}$$

is called the Schrödinger-equivalent potential. The exact expressions of $\mathcal{V}_e(k;\omega)$ and of $\mathcal{W}_e(k;\omega)$ given in Ref. 2 will be used in all the numerical calculations [Eqs. (5.1a) and (5.1b)]. For simplicity, here we only give their following approximate forms:

$$\mathcal{V}_e(k;\omega)\approx\mathcal{V}_\sigma(k;\omega)+\mathcal{V}_0(k;\omega)+\frac{\omega}{m}\mathcal{V}_0(k;\omega)\ , \tag{2.5a}$$

$$\mathcal{W}_e(k;\omega)\approx\mathcal{W}_\sigma(k;\omega)+\mathcal{W}_0(k;\omega)\ . \tag{2.5b}$$

If one omits $\mathcal{W}_e(k;\omega)$ in Eq. (2.4), the resulting relation

$$k^2+2m\mathcal{V}_e(k;\varepsilon)\approx\varepsilon^2+2m\varepsilon \tag{2.6}$$

defines a real function $k(\varepsilon)$; here and later, we use the notation ε rather than ω whenever the frequency and the momentum are related by Eq. (2.6), i.e., when ω is "on the energy shell." Later, we shall deal with quantities that depend upon only one variable, namely the nucleon momentum k or the nucleon energy ε, rather than upon both the momentum and the frequency. This is related to a quasiparticle approximation, as we now briefly recall. The dependence of the mean field upon ω reflects the fact that if one adds a nucleon with momentum k to the ground state one does not obtain a stationary state: indeed, this configuration is spread over many energy eigenstates. This spreading is described by a spectral function. That function has a peak near the quasiparticle energy $\varepsilon(k)$, which is determined by the energy-momentum relation (2.6). The Lorentz components of the mean field associated with a nucleon with momentum k is determined by the "on-the-energy-shell" value

$$V_\tau(k)=\mathcal{V}_\tau[k;\varepsilon(k)],\quad \tau=\sigma,0\ .$$

Equivalently, one can use Eq. (2.6) to express k as a function $k(\varepsilon)$ and write the on-the-energy-shell value as a function of the energy variable $V_\tau(\varepsilon)=\mathcal{V}_\tau[k(\varepsilon);\varepsilon]$.

The nonrelativistic mean field that is derived from phenomenological shell-model and optical-model analyses of the experimental data can be identified with the following quantity:

$$U_e(\varepsilon)=V_e(\varepsilon)+iW_e(\varepsilon)\ , \tag{2.7}$$

with

$$V_e(\varepsilon)=\mathcal{V}_e(k(\varepsilon);\varepsilon),\quad W_e(\varepsilon)=\mathcal{W}_e(k(\varepsilon);\varepsilon)\ . \tag{2.8a}$$

In keeping with the preceding paragraph, we shall also use the notation ($\tau=\sigma,0$)

$$\begin{aligned}&V_\tau(\varepsilon)=\mathcal{V}_\tau(k(\varepsilon);\varepsilon),\quad W_\tau(\varepsilon)=\mathcal{W}_\tau(k(\varepsilon);\varepsilon)\ ,\\ &V_\tau(k)=\mathcal{V}_\tau(k;\varepsilon(k)),\quad W_\tau(k)=\mathcal{W}_\tau(k;\varepsilon(k))\ .\end{aligned} \tag{2.8b}$$

B. Parametrization

The values of $W_\tau(\varepsilon)$, $\tau=\sigma,0$, calculated by ter Haar and Malfliet[4] in the framework of the relativistic BHF approximation are represented by the squares in Fig. 1. They can be approximated by the following parametric expression, first proposed by Brown and Rho[5] (BR) in the nonrelativistic case

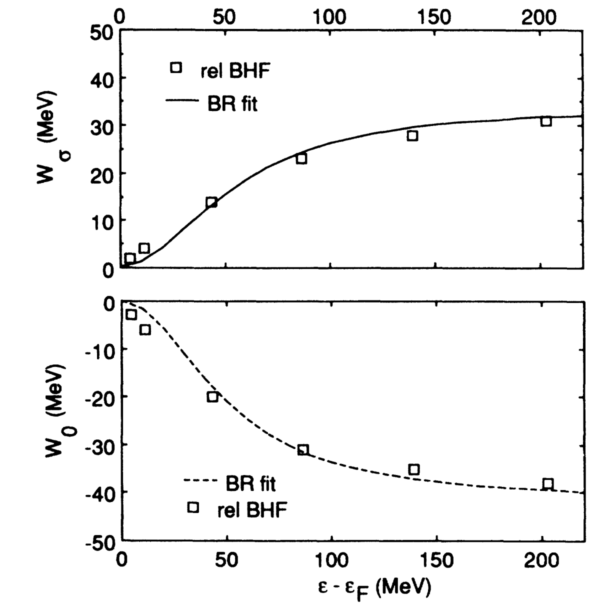

FIG. 1. Energy dependence of the imaginary parts of the scalar (top) and vector (bottom) Lorentz components of the mean field for $k_F=1.33\ \text{fm}^{-1}$. The squares represent the values calculated by ter Haar and Malfliet from the relativistic BHF approximation. The curves represent the parametrization given by Eqs. (2.9a) and (2.9b).

$$W_\tau^{\mathrm{BR}}(\varepsilon)=b_\tau\frac{(\varepsilon-\varepsilon_F)^2}{(\varepsilon-\varepsilon_F)^2+r_\tau^2}\ . \tag{2.9a}$$

The Fermi energy $\varepsilon_F=-17.4$ MeV has been calculated self-consistently from the values of $V_e(\varepsilon)$, which will be constructed in Sec. IV later. The curves drawn in Fig. 1 correspond to the following parameter values:

$$\begin{aligned}&b_\sigma=34\ \text{MeV},\quad r_\sigma=54.8\ \text{MeV}\ ,\\ &b_0=-42\ \text{MeV},\quad r_0=50.0\ \text{MeV}\ .\end{aligned} \tag{2.9b}$$

III. DISPERSIVE CORRECTIONS

We closely follow the analysis and terminology adopted in the nonrelativistic case.[6] We write each Lorentz component of the mean field in the following form:

$$\mathcal{V}_\tau(k;\omega)=\mathcal{V}_\tau(k;\varepsilon_F)+\Delta\mathcal{V}_\tau(k;\omega)\ . \tag{3.1}$$

The quantity $\mathcal{V}_\tau(k;\varepsilon_F)$ is independent of the frequency ω; its momentum dependence derives from spatial nonlocality. It is thus similar to the mean field encountered in the Hartree-Fock approximation. We thus call it the Hartree-Fock type (HF) contribution to the Lorentz component $\mathcal{V}_\tau$ and write it in the form

$$\mathcal{V}_\tau(k;\varepsilon_F)=V^{\mathrm{HF}}(\varepsilon)\ , \tag{3.2}$$

where we use Eq. (2.6) to express k in terms of ε.

The quantity $\Delta\mathcal{V}_\tau$ is connected to the imaginary part $\mathcal{W}_\tau$ by a dispersion relation,[2] that we write here in the subtracted form:

$$\Delta\mathcal{V}_\tau(k;\omega)=\frac{1}{\pi}\int \mathcal{W}_\tau(k;\omega')\left[\frac{1}{\omega'-\omega}-\frac{1}{\omega'-\varepsilon_F}\right]d\omega' , \tag{3.3}$$

where the integral is a principal value. It is called the dispersive contribution.[6] Its dependence upon k is expected to be quite smooth, since it is associated with spatial nonlocality. In contrast, its dependence upon ω is strong for ω close to ε_F where the quantity $\mathcal{W}_\tau(k;\omega')$ rapidly vanishes as $(\omega'-\varepsilon_F)^2$. Accordingly, we retain this main feature of $\mathcal{W}_\tau(k;\omega')$ and assume that this quantity is independent of k. In practice, this implies that the effect of the smooth k dependence of $\mathcal{W}_\tau$ is incorporated into the HF component. Here, we thus take $\mathcal{W}_\tau(k;\omega')\approx W_\tau(\omega')$. Furthermore, we replace the right-hand side of the latter approximation by the BR parametrization of Eqs. (2.9a) and (2.9b).

In summary, we write

$$\mathcal{V}_\tau(k;\varepsilon)=V_\tau^{\mathrm{HF}}(k)+\Delta V_\tau(\varepsilon) , \tag{3.4}$$

with

$$\Delta V_\tau(\varepsilon)=\frac{1}{\pi}\int_{\varepsilon_F}^{\infty} W_\tau^{\mathrm{BR}}(\varepsilon')\left[\frac{1}{\varepsilon'-\varepsilon}-\frac{1}{\varepsilon'-\varepsilon_F}\right]d\varepsilon' . \tag{3.5}$$

The fact that the integral runs only over values of ε' larger than ε_F is characteristic of the BHF approximation; we return to this point in Sec. VII.

The BR parametrization presents the practical advantage that the dispersive contribution can be evaluated in closed form.[7] Its scalar and vector components are plotted in Fig. 2. Equation (2.5a) shows that, for $\varepsilon/m \ll 1$, the quantity of physical interest is the sum

$$\Delta V(\varepsilon)=\Delta V_\sigma(\varepsilon)+\Delta V_0(\varepsilon) , \tag{3.6}$$

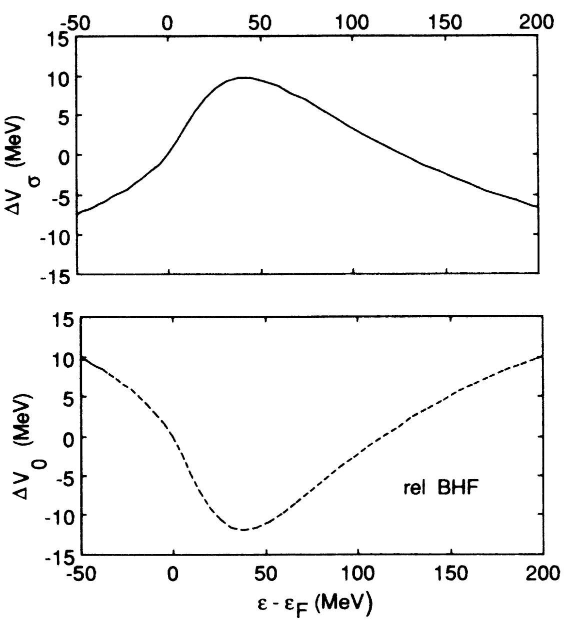

FIG. 2. Energy dependence of the dispersive contributions to the scalar and vector Lorentz components of the mean field, as evaluated from Eq. (3.5).

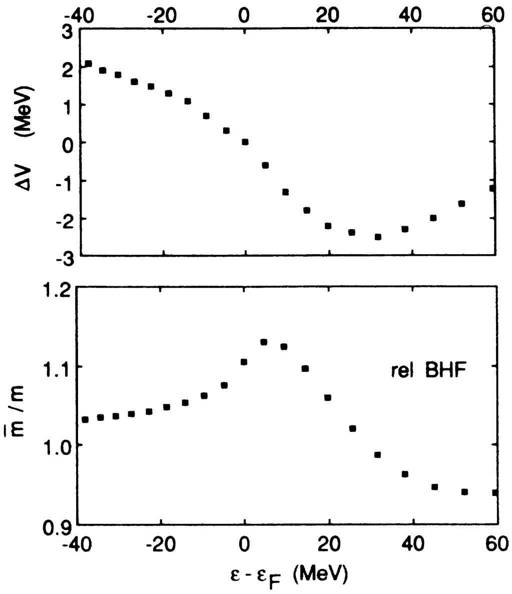

FIG. 3. Energy dependence of the total dispersive contribution ΔV (top) and of the corresponding E mass $\overline{m}/m$ (bottom).

which is plotted in the upper part of Fig. 3. Its energy dependence can be characterized by the following "E mass:"

$$\overline{m}(\varepsilon)/m=1-\frac{d}{d\varepsilon}\Delta V(\varepsilon) , \tag{3.7}$$

which is shown in the lower part of Fig. 3. The E mass has a vertical slope at $\varepsilon=\varepsilon_F$ and presents a maximum for ε slightly larger than ε_F. These properties are qualitatively similar to those encountered in the nonrelativistic BHF approximation;[8,9] in the latter case, however, the maximum of $\overline{m}/m$ reaches a sizably larger value (≈ 1.5); we return to this difference in Sec. VI. The value of $\overline{m}(\varepsilon)/m$ results from a cancellation between the energy derivatives of the scalar and vector parts. This is exhibited in Fig. 4, which shows the quantities

$$\overline{m}_\sigma(\varepsilon)/m=1-\frac{d}{d\varepsilon}\Delta V_\sigma(\varepsilon);\quad \overline{m}_0(\varepsilon)/m=1-\frac{d}{d\varepsilon}\Delta V_0(\varepsilon) . \tag{3.8}$$

In Fig. 4, we used k/k_F as a variable in order to facilitate comparison with results previously obtained from the nonrelativistic BHF approximation: in Eq. (3.8), we changed, the dependence upon ε into a dependence upon k by using Eq. (2.6).

IV. HARTREE-FOCK TYPE CONTRIBUTION

In Eq. (3.4), we expressed the real part of each Lorentz component as the sum of a dispersive and a HF contribution. The former has been calculated in Sec. III; we now evaluate the HF contribution. The k dependence of the HF contribution reflects the nonlocality of each Lorentz component. We thus parametrize it as a Gaussian, in keeping with the Perey-Buck model of nonlocality:[10]

$$V_\tau^{\mathrm{HF}}(k)=v_\tau\exp(-\tfrac{1}{4}\mu_\tau^2k^2) ; \tag{4.1}$$

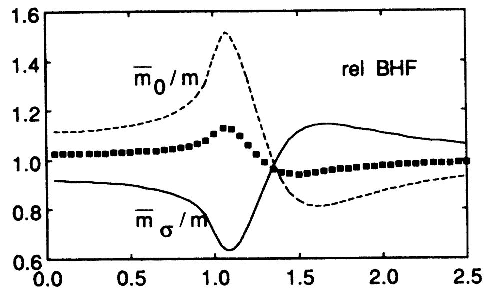

FIG. 4. Dependence upon k/k_F of the E masses associated with the scalar component (solid curve) and with the vector component (dashed line). The solid squares represent the same total E mass as in Fig. 3.

μ_τ is the range of nonlocality. We relate ε to k via Eq. (2.6) and write the full real part in the form

$$V_\tau(k)=V_\tau^{\rm HF}(k)+\Delta V_\tau(k)\ ; \tag{4.2}$$

as in Eq. (2.8b), we use the same symbol to denote V_τ when expressed as a function of either k or ε; this notation will also be used below for other quantities.

The parametrization (4.1) involves two parameters, namely v_τ and μ_τ. We determine them by fitting the results calculated for $V_\tau(k)$ by ter Haar and Malfliet in their relativistic BHF approximation. These values are represented by the squares in Fig. 5. There, the solid curves show the fits obtained by adding $\Delta V_\tau(k)$ to the HF contribution [Eq. (4.1)] for the following parameter values:

$$\begin{aligned} v_\sigma&=-417\ \text{MeV},\quad \mu_\sigma=0.35\ \text{fm}\ ,\\ v_0&=340\ \text{MeV},\quad \mu_0=0.40\ \text{fm}\ . \end{aligned} \tag{4.3}$$

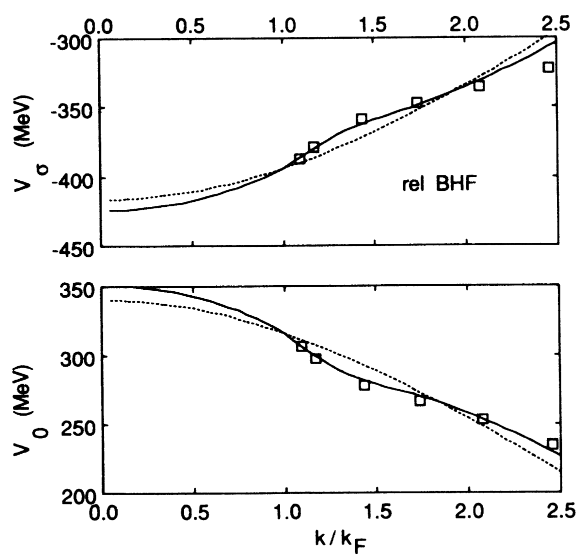

FIG. 5. Dependence upon k/k_F of the scalar (top) and vector (bottom) components of the real part of the relativistic mean field. The squares represent the values calculated by ter Haar and Malfliet (Table 4.2 of Ref. 4). The dashed curves give the HF contribution [Eqs. (4.1) and (4.3)]. The solid lines show the full real part [Eq. (4.2)].

The fits can be considered as quite satisfactory in view of the simple nature of our parametrization. It is particularly noteworthy that the fits reproduce the wiggle of $V_\sigma(k)$ and of $V_0(k)$ for k somewhat larger than k_F.

V. EFFECTIVE MASSES

We are now in a position to evaluate various effective masses that have been defined in Ref. 2. We first recall the exact expressions of the real part of the Schrödinger-equivalent potential defined by Eqs. (2.2)–(2.4):

$$\mathcal{V}_e(k\,;\omega)=\mathcal{Y}_e(k\,;\omega)+\frac{\omega}{m}\mathcal{V}_0(k\,;\omega)\ , \tag{5.1a}$$

$$\mathcal{Y}_e(k\,;\omega)=\mathcal{V}_\sigma(k\,;\omega)+\mathcal{V}_0(k\,;\omega)+\frac{1}{2m}(\mathcal{V}_\sigma^2-\mathcal{V}_0^2-\mathcal{W}_\sigma^2+\mathcal{W}_0^2)\ . \tag{5.1b}$$

The "k mass" $\tilde{m}$ is defined by

$$\tilde{m}(\varepsilon)/m=\left[1+\frac{m}{k}\frac{\partial}{\partial k}\mathcal{V}_e(k\,;\varepsilon)\right]^{-1}_{k=k(\varepsilon)}\ , \tag{5.2}$$

where $k(\varepsilon)$ is given by Eq. (2.6). The k mass describes the fact that the microscopic potentials $\mathcal{U}_\sigma(k\,;\omega)$ and $\mathcal{U}_0(k\,;\omega)$ are k dependent, or equivalently that their Fourier transforms are nonlocal in the spatial coordinates. In our approach this dependence is contained in the HF contribution [Eq. (3.4)]. The calculated value of $\tilde{m}/m$ is represented by the short dashes in Fig. 6. In contrast to the nonrelativistic BHF approximation, $\tilde{m}$ is larger than m because the nonlocality of $\mathcal{V}_e$ results from a combination of the nonlocality of $\mathcal{V}_\sigma$ and that of $\mathcal{V}_0$.[2]

The "E mass" is defined by

$$\overline{m}(\varepsilon)/m=1-\left[\partial\mathcal{Y}_e(k\,;\varepsilon)/\partial\varepsilon+\frac{\varepsilon}{m}\partial\mathcal{V}_0(k\,;\varepsilon)/\partial\varepsilon\right]_{k=k(\varepsilon)}\ . \tag{5.3}$$

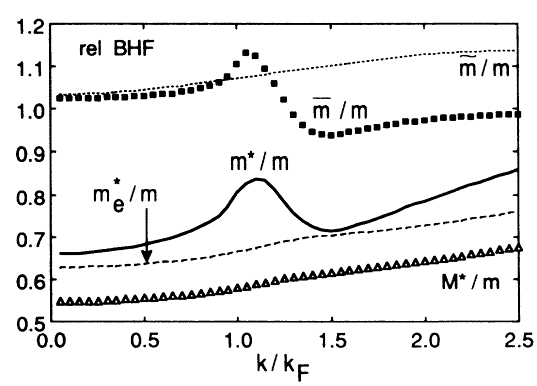

FIG. 6. Dependence upon k/k_F of the k mass $\tilde{m}/m$ (short-dashed line), of the E mass $\overline{m}/m$ (solid squares), of the Lorentz mass m_e^*/m (long-dashed line), of the Dirac mass M^*/m (triangles) and of the nonrelativistic-type effect mass m^*/m (solid curve), as derived from our analysis of the relativistic BHF approximation.

It derives from the frequency dependence of the microscopic fields $\mathcal{V}_\sigma$ and $\mathcal{V}_0$, or equivalently of the fact that their Fourier transforms are nonlocal in the time coordinate. This is often referred to as a "retardation effect" in the terminology used in relativistic approaches.[11] The E mass calculated from Eq. (5.3) is represented by the solid squares in Fig. 6; it is numerically very close to the approximation used in the lower part of Fig. 3.

The "Lorentz mass" m_e^* is defined by

$$m_e^*(\varepsilon)/m = 1 - \frac{1}{m} V_0(\varepsilon) . \tag{5.4}$$

It derives from the fact that $\mathcal{V}_\sigma$ and $\mathcal{V}_0$ have different Lorentz transformation properties. It does not appear in a nonrelativistic approach. It is represented by the long dashes in Fig. 6.

The "Dirac mass" M^* is defined by

$$M^*(\varepsilon)/m = 1 + \frac{1}{m} V_\sigma(\varepsilon) ; \tag{5.5}$$

this quantity is often called the effective mass in relativistic approaches. It is represented by the triangles in Fig. 6. It is equal to 0.58 at the Fermi energy; this is identical to the optimal value of M^* determined by Rufa *et al.*[12] from extended fits to the experimental nuclear ground-state properties.

The quantity that should be identified with the effective mass derived from nonrelativistic shell-model and optical-model analyses is the "nonrelativistic-type effective mass" m^* which is defined as follows:

$$m^*(\varepsilon)/m = 1 - \frac{d}{d\varepsilon} V_e(\varepsilon) , \tag{5.6}$$

where $V_e(\varepsilon)$ is the real part of the Schrödinger-equivalent potential. The quantity m^*/m is represented by the solid curve in Fig. 6. It is equal to 0.80 at the Fermi energy, where it has a vertical slope; it reaches a maximum, equal to 0.84, at $k = 1.12 k_F$. This enhancement of the nonrelativistic-type effective mass near the Fermi energy constitutes the "Fermi surface anomaly."

Figure 7 shows that this anomaly is nearly the same in the relativistic as in the nonrelativistic BHF approximation.[13] We now discuss the similarities and differences between the two approaches. In the relativistic BHF approximation, the quantities m^*, $\tilde{m}$, m_e^*, and $\overline{m}$ are related by an identity [Eq. (4.17) of Ref. 2] that can accurately be approximated as follows:

$$\frac{m^*(\varepsilon)}{m} \approx \frac{\tilde{m}(\varepsilon)}{m} \left[\frac{m_e^*(\varepsilon)}{m} + \frac{\overline{m}(\varepsilon)}{m} - 1 \right] . \tag{5.7}$$

The quantities $\tilde{m}$ and m_e^* are smooth monotonic functions of ε. Hence, the Fermi surface anomaly is due to the E mass that derives from the dispersive contribution. The latter arises from the coupling of the single-particle degree of freedom with two particle-one hole excitations of the Fermi sea. In the nonrelativistic case, one also introduces a k-mass ($\tilde{m}_{nr}$) to characterize the spatial nonlocality of the potential and a E mass ($\overline{m}_{nr}$) to characterize its frequency dependence.[8] Their relation to the nonrelativistic effective mass m^*_{nr} is the following:

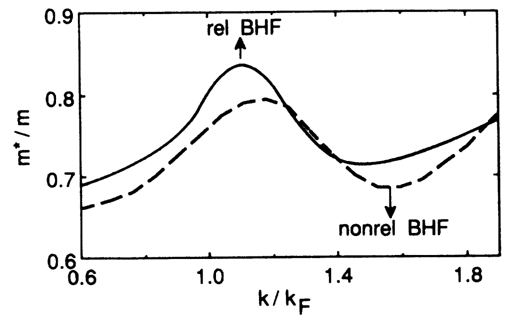

FIG. 7. The solid curve is the effective mass determined from our analysis of the relativistic BHF calculation of ter Haar and Malfliet (Ref. 4) for $k_F = 1.33$ fm^{-1}. The dashed curve represents the effective mass calculated from the nonrelativistic BHF calculation by Baldo *et al.* (Ref. 13) for $k_F = 1.44$ fm^{-1}; these authors used as input a separable form of the Paris nucleon-nucleon interaction.

$$\frac{m^*_{nr}(\varepsilon)}{m} = \frac{\tilde{m}_{nr}(\varepsilon)}{m} \cdot \frac{\overline{m}_{nr}(\varepsilon)}{m} . \tag{5.8}$$

The k mass $\tilde{m}_{nr}(\varepsilon)$ is a smooth monotonic function of ε; it is similar to the Lorentz mass, but the latter does not appear in the nonrelativistic case. The Fermi-surface anomaly is thus due to $\overline{m}_{nr}(\varepsilon)$, which results from the dispersive effects as in the relativistic case. The peak of $\overline{m}$ is more pronounced in the nonrelativistic than in the relativistic case. However, its influence on m^* is damped in the nonrelativistic case because in Eq. (5.8) $\overline{m}_{nr}(\varepsilon)$ is multiplied by $\tilde{m}_{nr}(\varepsilon)$, which is close to 0.6 near the Fermi surface.[8]

VI. OCCUPATION PROBABILITIES

In second order in the Brueckner reaction matrix, the depletion of the Fermi sea is represented by the Goldstone diagram on the left-hand side of Fig. 8.[14] This diagram accounts for the fact that two nucleons with momenta $h, h' < k_F$ can interact and acquire momenta $p', p'' > k_F$. As a consequence, the momentum state $h < k_F$ is partly empty. The corresponding occupation probability of the hole momentum h is given by

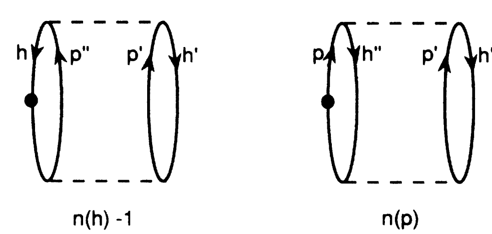

FIG. 8. The diagram on the left-hand side describes the lowest-order contribution to the depletion of the Fermi sea. The diagram on the right-hand side describes the lowest-order contribution to the population of states with momentum $p > k_F$. Upward pointing arrows correspond to particle states ($p, p', p'' > k_F$) and downward pointing arrows to hole states ($h, h', h'' < k_F$); the primed labels are summed over. The horizontal dashed lines represent reaction matrices.

$$n(h)=\left[1+\frac{d}{d\varepsilon}V_\sigma(\varepsilon)+\frac{d}{d\varepsilon}V_0(\varepsilon)\right]_{\varepsilon=\varepsilon(h)}$$

$$=3-\frac{\overline{m}_\sigma(h)}{m}-\frac{\overline{m}_0(h)}{m}\ , \tag{6.1}$$

where $\varepsilon(h)$ is defined by Eq. (2.6). The quantities $\overline{m}_\sigma(h)$ and $\overline{m}_0(h)$ have been defined in Eq. (3.8) and plotted in Fig. 4. The occupation probability calculated from Eq. (6.1) is represented by the solid curve in Fig. 9. The amount of depletion of the Fermi sea can conveniently be measured by the quantity

$$\kappa=1-\frac{3}{k_F^3}\int_0^{k_F}n(h)h^2dh\ . \tag{6.2}$$

Our calculation yields $\kappa=0.05$. In the relativistic BHF approximation, the depletion of the Fermi sea thus amounts to about five percent. This is sizably smaller than the value obtained in the case of the nonrelativistic BHF approximation:[9,15] the dashed curve in Fig. 9 yields $\kappa_{nr}=0.25$ (the value of κ_{nr} is somewhat smaller if one uses as input a nucleon-nucleon interaction with a weaker tensor component,[8,16] but it remains close to 0.20). One could wonder whether the large difference between the values of κ obtained from the relativistic and nonrelativistic approaches might not be due to our approximations, in particular to our neglect of the k dependence of $\mathcal{W}_\tau(k;\omega)$ or to the possibility that the BR parametrization becomes inaccurate for large energies. We do not believe that this is plausible. For instance, if one would arbitrarily increase by 100% (8 MeV) our input value of $W_\sigma(\varepsilon)+W_0(\varepsilon)$ for $\varepsilon>500$ MeV, this would yield to increase κ by only 0.005. Hence, we trust that our evaluation of κ is accurate within about 0.02, and that the predicted depletion of the Fermi sea is indeed much smaller in the relativistic than in the nonrelativistic approach.

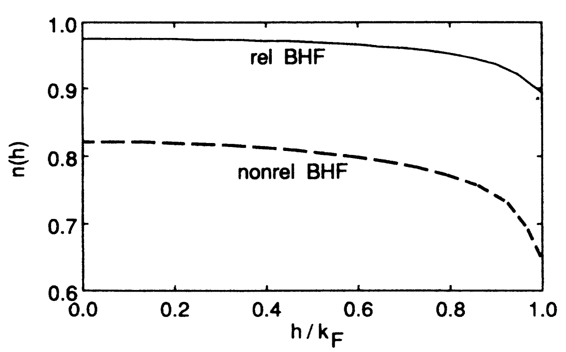

FIG. 9. Momentum distribution below the Fermi surface. The solid curve corresponds to the relativistic BHF approximation ($k_F=1.33$ fm^{-1}). The dashed line has been obtained from the nonrelativistic BHF approximation ($k_F=1.36$ fm^{-1}), using as input the same Paris nucleon-nucleon interaction as for the dashed line in Fig. 7 (Ref. 15).

VII. CORRELATION AND RENORMALIZATION CORRECTIONS

The nonrelativistic BHF approximation is the leading term of a hole-line expansion whose rate of convergence is determined by the size of κ. Among the corrections to the BHF approximation to the mean field, let us consider those that are represented by the graphs of Fig. 10 in which we take $p>k_F$ for definiteness. The graph labeled CO is called the correlation contribution, because it accounts for the fact that the addition of the nucleon p to the correlated ground state is inhibited since this momentum state is partly occupied. This CO contribution is thus intimately related to the occupation probability $n(p)$ (compare the right-hand side of Fig. 8 with the left-hand side of Fig. 10), as we now describe.

Let us denote by $\mathcal{V}^{CO}(k;\omega)+i\mathcal{W}^{CO}(k;\omega)$ the contribution of the graph CO to the nonrelativistic mass operator. These quantities are connected by a dispersion relation:[6]

$$\mathcal{V}^{CO}(k;\omega)=\frac{1}{\pi}\int_{-\infty}^{\varepsilon_F}\frac{\mathcal{W}^{CO}(k;\omega')}{\omega'-\omega}d\omega'\ , \tag{7.1}$$

where we took into account that $\mathcal{W}^{CO}(k;\omega')$ vanishes for $\omega'>\varepsilon_F$. The integral converges because $\mathcal{W}^{CO}(k;\omega')$ is equal to zero for large negative ω', because of momentum conservation.[18] The occupation probability for particle momenta can be approximated by[8]

$$n_{nr}(p)=-\left[\frac{\partial}{\partial\omega}\mathcal{V}^{CO}(p;\omega)\right]_{\omega=\varepsilon(p)}\ , \tag{7.2a}$$

where $\varepsilon(p)$ is defined by Eq. (2.6). The extension of these relations to the relativistic is straightforward: add an index τ ($\tau=\sigma,0$) to $\mathcal{V}^{CO}$ and $\mathcal{W}^{CO}$, use Eq. (7.1) for each of these Lorentz components, and replace Eq. (7.2a) by

$$n(p)=-\left\{\frac{\partial}{\partial\omega}\left[\mathcal{V}_\sigma^{CO}(p;\omega)+\mathcal{V}_0^{CO}(p;\omega)\right]\right\}_{\omega=\varepsilon(p)}\ . \tag{7.2b}$$

The quantities $W_\sigma^{CO}(\varepsilon), W_0^{CO}(\varepsilon)$ have recently been evaluated in the framework of Walecka's model Lagrangian,[17] but no information is available in the case of the

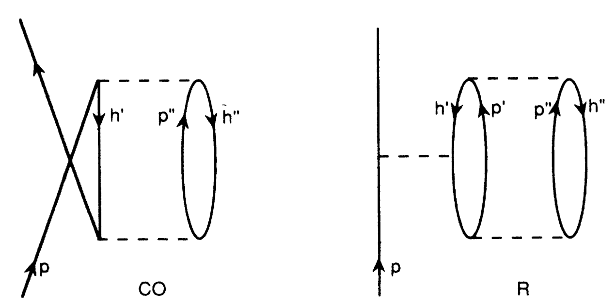

FIG. 10. Corrections to the BHF approximation to the mean field. The diagram labeled CO corresponds to the correlation contribution. The "renormalization" contribution is represented by the diagram labeled R.

Bruekner expansion. We thus consider the following crude model. For ω close to ε_F, the quantities $\mathcal{W}_\tau^{\rm CO}(k;\omega)$ vanish like $(\omega-\varepsilon_F)^2$. For k close to k_F, they vanish for $\omega < -7\varepsilon_F = -122$ MeV, because of momentum conservation.[18] In keeping with these properties we assume that $\mathcal{W}_\tau^{\rm CO}(k;\omega)$ is independent of k. We take it equal to $NW_\tau(\omega)$ where N is a normalization factor; $W_\tau(\omega)$ is set equal to zero for $\omega < -100$ MeV and is chosen equal to the value given by Eqs. (2.9a) and (2.9b) for -100 MeV $< \omega < \varepsilon_F$. We calculate $n(p)$ from Eq. (7.2b) and determine the normalization factor N in such a way that the sum rule

$$\int_0^\infty n(k)k^2dk = \tfrac{1}{3}k_F^3 \qquad (7.3)$$

is fulfilled; this yields $N=0.5$. The value of $n(p)$ calculated from this crude model is represented by the solid curve in Fig. 11. There, the dashed line represents the result obtained from the nonrelativistic expression of the correlation diagram,[15] using the same input as for the dashed line in Fig. 9. The occupation probability of particle states ($p > k_F$) is seen to be much larger in the nonrelativistic than in the relativistic approach; this was expected from Fig. 9 and Eq. (7.3) and should persist in a more realistic model.

Our model enables one to calculate the contribution of the correlation diagram to the Schrödinger-equivalent potential, namely ($\varepsilon/m \ll 1$)

$$V_e^{\rm CO}(\varepsilon) \approx V_\sigma^{\rm CO}(\varepsilon) + V_0^{\rm CO}(\varepsilon) . \qquad (7.4)$$

This quantity is plotted in the upper part of Fig. 12. It is equal to 1.2 MeV at the Fermi surface. This is much smaller than the depth $V_e(\varepsilon_F) = -54.6$ MeV of the Schrödinger-equivalent potential as calculated in the BHF approximation. This is in striking contrast with the situation encountered in the nonrelativistic approach, in which the correlation correction is as large as $+10$ MeV.[9,13]

The correlation contribution contributes to the E mass. The full E mass reads ($\varepsilon/m \ll 1$)

$$\overline{m} = \overline{m}_{\rm BHF} + \overline{m}_{\rm CO} - m , \qquad (7.5)$$

where $\overline{m}_{\rm BHF}$ is the E mass calculated from the relativistic BHF approximation, while

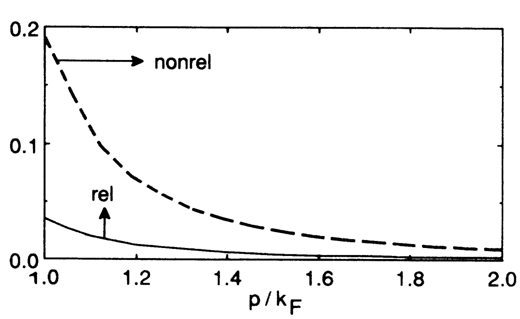

FIG. 11. Momentum distributions for $p > k_F$. The solid curve has been calculated from the relativistic model described in Sec. VII. The dashed line has been calculated (Ref. 15) from the nonrelativistic expression of the graph CO, using the same input Paris nucleon-nucleon interaction as in Fig. 9.

$$\overline{m}_{\rm CO}(\varepsilon)/m = 1 - \frac{d}{d\varepsilon} V^{\rm CO}(\varepsilon) . \qquad (7.6)$$

These quantities are represented in the lower part of Fig. 12. It is seen that the correlation contribution barely modifies the BHF value of the E mass above the Fermi surface. Correspondingly, it hardly modifies the BHF value for the effective mass $m^*(\varepsilon)$.

Another correction to the BHF approximation is represented by the graph labeled R in Fig. 10; in the *nonrelativistic* terminology, it is called the "renormalization" correction: when added to the BHF approximation it yields the "renormalized BHF approximation." It accounts for the fact that the nucleon with momentum p cannot interact with the hole labeled h' whenever the latter hole state is empty. Its contribution to $V_e(\varepsilon)$ can be approximated by

$$R(\varepsilon) \approx -\kappa V_e^{\rm BHF}(\varepsilon) , \qquad (7.7)$$

where κ is the depletion parameter and $V_e^{\rm BHF}(\varepsilon)$ is the BHF value. In the relativistic case, this yields $R(\varepsilon_F) \approx 2.8$ MeV. This is much smaller than the value $R_{\rm nr}(\varepsilon_F) \approx 13$ MeV obtained in the nonrelativistic case.[15]

The Hugenholtz-Van Hove theorem[19] states that for nuclear matter at equilibrium the Fermi energy ε_F is equal to the average binding energy per nucleon. In the nonrelativistic BHF approximation, this theorem is violated by as much as 15 MeV, which is approximately

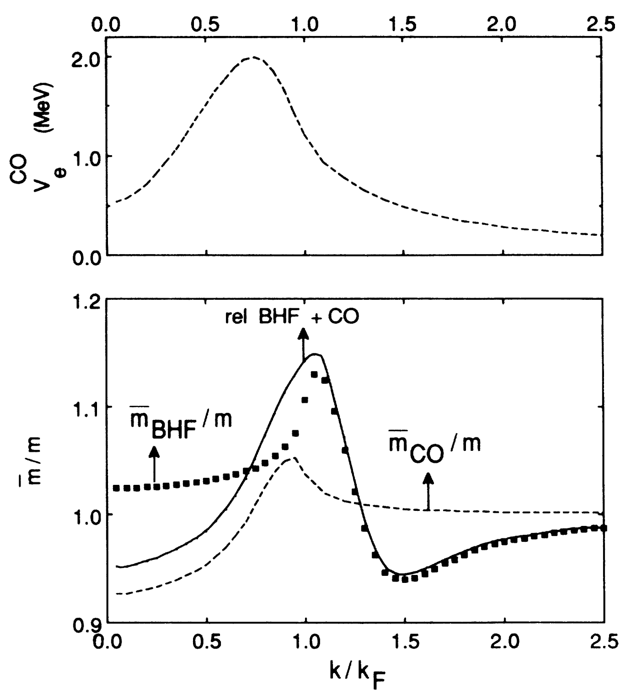

FIG. 12. The upper part gives the correlation contribution to the Schrödinger-equivalent potential, as evaluated from the model described in Sec. VII [Eq. (7.4)]. The lower part shows the E mass as calculated in the relativistic BHF approximation (solid squares, see Fig. 6), the quantity $\overline{m}_{\rm CO}/m$ [dashed line, Eq. (7.6)], and the full E mass (solid curve) associated with the sum of the relativistic BHF and correlation contributions.

explained by the large value of the diagrams CO and R of Fig. 10.[8,9,13] Malfliet[1] recently pointed out that, in the relativistic BHF approximation, the violation of the Hugenholtz-Van Hove theorem amounts to only 4 MeV; he thus conjectured that the corrections to the BHF approximation are smaller in the relativistic than in the nonrelativistic case. This is fully confirmed by our present results.

VIII. SUMMARY AND DISCUSSION

In first approximation, the potential energy of a nucleon is a linear function of energy up to about 100 MeV; this is found, for instance, in the Hartree-Fock approximation to the mean field. When one takes into account the possibility of exciting the Fermi sea, four new features appear. (i) The mean field acquires an imaginary part above the Fermi energy. (ii) The energy derivative of its real part varies rapidly in the vicinity of the Fermi surface: this constitute the Fermi surface anomaly. (iii) The mean field depends upon the nucleon frequency in addition to its momentum; this frequency dependence reflects dispersive or retardation effects. (iv) The Fermi sea is partly depleted. These four features are common to the relativistic and nonrelativistic descriptions of the mean field.[2,20] Our main purpose was to perform their quantitative investigation in the framework of the relativistic BHF approximation.

Our basic procedure consisted in writing the real part $\mathcal{V}_\tau(k;\omega)$ of each Lorentz component ($\tau=\sigma,0$) as the sum of a HF contribution that is a smooth function of the nucleon momentum k, and of a dispersive contribution that is a function of the frequency ω and contains the retardation effects [Eq. (3.4)]. We evaluated the dispersive contribution from a subtracted dispersion relation [Eq. (3.5)] using as input the imaginary part of the mean field calculated by ter Haar and Malfliet[4] from the relativistic BHF approximation. Above 150 MeV, the absolute value of the imaginary Lorentz components $\mathcal{W}_\tau(\omega)$ is fairly independent of frequency, but it rapidly decreases near the Fermi energy ε_F, where it vanishes like $(\omega-\varepsilon_F)^2$, see Fig. 1. The dispersion relation implies that this rapid decrease is accompanied by a rapid energy dependence of the frequency derivative of $\Delta V_\tau(\omega)$ for ω near ε_F (Figs. 2 and 3). This is conveniently characterized by the E mass $\overline{m}/m$ (Fig. 4); the latter also plays an important role in the determination of the depletion of the Fermi sea [Eq. (6.1)].

In practice, one is mainly interested in the on-the-energy-shell values of the various quantities, i.e., those values in which Eq. (2.6) is used to relate the momentum and the frequency. In our approach, the on-the-energy-shell quantity $V_\tau(\varepsilon)$ is the sum of a HF and of a dispersive contribution [Eq. (4.2)]. The latter is known from the dispersion relation. The former has been approximated by a Gaussian [Eq. (4.1)] whose parameters have been determined by fitting the values of V_τ calculated by ter Haar and Malfliet[4] (Fig. 5). This procedure yields an algebraic expression for $V_\tau(\varepsilon)$, from which energy derivatives can then conveniently be evaluated. This is of practical interest because these derivatives rapidly depend upon energy in the vicinity of the Fermi surface; this "Fermi surface anomaly" would be difficult to investigate directly since this would require an accurate determination of the energy derivative of potentials computed at discrete energies from a relativistic BHF program. The same difficulty has been encountered in the nonrelativistic case, where it has been overcome in a similar way as here.[20]

In order to compare the relativistic and nonrelativistic BHF results, it is convenient to consider the Schrödinger-type potential energy $V_e(\varepsilon)$, which can be approximated by

$$V_\sigma(\varepsilon)+(1+\varepsilon/m)V_0(\varepsilon)\ .$$

The nonrelativistic-type effective mass

$$m^*(\varepsilon)/m=1-dV_e(\varepsilon)/d\varepsilon$$

is the quantity that should be compared with the effective mass derived from nonrelativistic shell-model or optical-model analyses of the experimental data. Figure 7 shows that the value of m^* determined in the present investigation is nearly the same as that calculated from the nonrelativistic BHF approximation. The effective mass m^* presents a maximum near the Fermi surface; this constitutes the Fermi surface anomaly. Figure 6 shows the various contributions to m^*, namely the k mass $\tilde{m}$, the E mass $\overline{m}$ and the Lorentz mass m_e^* [Eq. (5.6)]; it is seen that the Fermi surface anomaly is due to the E mass, which is the quantity that describes the dispersive or retardation effects. The anomaly would have been very difficult to investigate in detail had we not first disentangled the momentum from the frequency dependence of $\mathcal{V}_\tau(k;\omega)$.

It was often believed that the relativistic approaches to the mean field yield too small values for the effective mass. We showed that this belief is ill founded. It had two main origins. First, many relativistic approaches do not include the dispersive effects. Second, some confusion exists because of the terminology. In relativistic approaches, the expression "effective mass" indeed usually denotes the Dirac mass $M^*(\varepsilon)=m+V_\sigma(\varepsilon)$. This quantity presents no maximum near the Fermi energy (Fig. 6). It is sizably smaller than m^*; as a matter of fact, the value of the Dirac mass at the Fermi energy is exactly equal to that determined in Ref. 12 from fits to various empirical properties of the nuclear ground states, namely $M^*(\varepsilon_F)/m\approx0.58$.

While the effective mass $m^*(\varepsilon)$ is nearly the same in the relativistic as in the nonrelativistic BHF approximation, the k mass and the E mass take very different values in the two cases. The large difference between the values found for the E mass in the relativistic and nonrelativistic BHF approximations reflects the difference between the dispersion relations that apply in the two cases.[2] It implies the existence of a large difference between the values predicted for the depletion of the Fermi sea (Fig. 9). The depletion parameter that measures the average probability of a whole momentum state being empty is found equal to 0.05 in the relativistic BHF approximation, while it is as large as 0.25 in the nonrelativistic BHF approximation. This strongly hints that the quantities called the "correlation" and "renormalization" corrections in the nonrelativistic terminology are much smaller in the relativistic than in the relativistic Brueckner expansion, since these corrections account for part of the effect of the depletion of the Fermi sea. This is confirmed in Sec. VII, where we constructed a crude model to evaluate these corrections and their influence on the effective mass (Fig. 12). Up to the Fermi energy, the sum of their contributions to the Schrödinger-type potential energy V_e is found equal to about $+4$ MeV; this is the magnitude of the correction needed to fulfill the Hugenholtz-Van Hove theorem.[1]

In summary, we investigated in detail the energy dependence of the mean field in the vicinity of the Fermi surface in the case of the relativistic BHF approximation. This energy dependence is conveniently described by the effective mass $m^*(\varepsilon)$, that we showed to be nearly the same in the relativistic as in the nonrelativistic BHF approximation. Consequently, this quantity cannot be used to distinguish between the two approaches. A more promising test appears to be provided by the depletion of the Fermi sea, which we found to be much smaller in the relativistic than in the nonrelativistic approach. At present, empirical information on this depletion is becoming available in the vicinity of the Fermi surface; there, however, a straightforward comparison with nuclear matter is delicate because the nuclear surface plays a dominant role.[20] Therefore, the comparison between empirical values and theoretical predictions should rather bear on the deeply bound shell model orbits, on which experimental results are forthcoming.[21,22]

We are very grateful to the authors of Ref. 15 for having provided the dashed curves in Figs. 9 and 11 prior to publication.

[1] R. Malfliet, in *Progress in Particle and Nuclear Physics,* edited by A. Faessler (Pergamon, New York, 1988). Vol. 21, p. 207.
[2] M. Jaminon and C. Mahaux, Phys. Rev. C **40**, 354 (1989).
[3] R. D. Lawson, P. T. Guenther, and A. B. Smith, Phys. Rev. C **34**, 1599 (1986).
[4] B. ter Haar and R. Malfliet, Phys. Rep. **149**, 207 (1987).
[5] G. E. Brown and M. Rho, Nucl. Phys. **A372**, 397 (1981).
[6] C. Mahaux and R. Sartor, Nucl. Phys. **A468**, 193 (1987).
[7] C. Mahaux and R. Sartor, Nucl. Phys. **A503**, 525 (1989).
[8] J.-P. Jeukenne, A. Lejeune, and C. Mahaux, Phys. Rep. **25**, 83 (1976).
[9] P. Grangé, J. Cugnon, and A. Lejeune, Nucl. Phys. **A473**, 365 (1987).
[10] F. G. Perey and B. Buck, Nucl. Phys. **32**, 353 (1962).
[11] J. Götz, J. Ramschütz, F. Weber, and M. K. Weigel, Phys. Lett. B **226**, 213 (1989).
[12] M. Rufa, P.-G. Reinhard, J. A. Maruhn, W. Greiner, and M. R. Strayer, Phys. Rev. C **38**, 390 (1988).
[13] M. Baldo, I. Bombaci, L. S. Ferreira, G. Giansiracusa, and U. Lombardo, Phys. Lett. B **209**, 135 (1988).
[14] D. J. Thouless, Rep. Prog. Phys. **27**, 53 (1964).
[15] M. Baldo, G. Giansiracusa, U. Lombardo, C. Mahaux, and R. Sartor (unpublished).
[16] S. Fantoni and V. R. Pandharipande, Nucl. Phys. **A427**, 473 (1984).
[17] M. H. Steffani, M. Betz, and Th. A. J. Maris, Nucl. Phys. **A493**, 493 (1989).
[18] R. Sartor and C. Mahaux, Phys. Rev. C **21**, 1546 (1980).
[19] N. M. Hugenholtz and L. Van Hove, Physica **24**, 363 (1958).
[20] C. Mahaux, P. F. Bortignon, R. A. Broglia, and C. H. Dasso, Phys. Rep. **120**, 1 (1985).
[21] P. K. A. de Witt Huberts, in *Electron-Nucleus Scattering,* edited by A. Fabrocini, S. Fantoni, S. Rosati, and M. Viviani (World Scientific, Singapore, 1989), p. 349.
[22] P. K. A. de Witt Huberts, in *Proceedings of the International Symposium on the Nuclear Shell Model,* edited by T.S.-Harry Lee and R. B. Wiringa (North-Holland, Amsterdam, 1989).